JGR Biogeosciences

RESEARCH ARTICLE
10.1029/2021JG006406

Special Section:
Advances in scaling and modeling of land-atmosphere interactions

Warming and Increased Respiration Have Transformed an Alpine Steppe Ecosystem on the Tibetan Plateau From a Carbon Dioxide Sink Into a Source

Hanbo Yun[1,2,3], Jing Tang[4], Ludovica D'Imperio[2], Xiaobo Wang[5], Yang Qu[6], Licheng Liu[7], Qianlai Zhuang[3], Wenxin Zhang[2,4], Qingbai Wu[1], Anping Chen[8], Qing Zhu[9], Deliang Chen[10], and Bo Elberling[2]

[1]State Key Laboratory of Frozen Soil Engineering, BeiLu'He Station, Northwest Institute of Eco–Environment and Resources, Chinese Academy of Sciences, Lanzhou, China, [2]Center for Permafrost (CENPERM), Department of Geosciences and Natural Resource Management, University of Copenhagen, Copenhagen, Denmark, [3]Department of Earth, Atmospheric and Planetary Sciences, Purdue University, West Lafayette, IN, USA, [4]Department of Physical Geography and Ecosystem Science, Lund University, Lund, Sweden, [5]Key Laboratory of Ecohydrology of Inland River Basin, Northwest Institute of Eco-Environment and Resources, Chinese Academy of Sciences, Lanzhou, China, [6]School of Urban and Regional Science, East China Normal University, Shanghai, China, [7]Department of Bioproducts and Biosystems Engineering, University of Minnesota, St Paul, MN, USA, [8]Department of Biology and Graduate Degree Program in Ecology, Colorado State University, Fort Collins, CO, USA, [9]Climate Sciences Department, Climate and Ecosystem Sciences Division, Lawrence Berkeley National Laboratory, Berkeley, CA, USA, [10]Department of Earth Sciences, University of Gothenburg, Gothenburg, Sweden

Abstract Cold region ecosystems store vast amounts of soil organic carbon (C), which upon warming and decomposition can affect the C balance and potentially change these ecosystems from C sinks to carbon dioxide (CO_2) sources. We quantified the decadal year-round CO_2 flux from an alpine steppe-ecosystem on the Tibetan Plateau using eddy covariance and automatic chamber approaches during a period of significant warming (0.13°C per 10 years; and 0.18°C in the non-growing season alone: 1st October to next 30th April). The results showed that ongoing climate change, mainly warming within the topsoil layers, is the main reason for the site's change from a sink for to a source of CO_2 in the atmosphere. Non-growing-season ecosystem respiration accounted for 51% of the annual ecosystem respiration and has increased significantly. The growing seasons (1st May to 30th September) were consistent CO_2 sink periods without significant changes over the study period. Observations revealed high-emission events from the end of the non-growing season to early in the growing season (1st March to fifteenth May), which significantly ($p < 0.01$) increased at a rate of 22.6 g C m^{-2} $decade^{-1}$, ranging from 14.6 ± 10.7 g C m^{-2} yr^{-1} in 2012 to 35.3 ± 12.1 g C m^{-2} yr^{-1} in 2017. Structural equation modeling suggested that active layer warming was the key factor in explaining changes in ecosystem respiration, leading to significant changes in net ecosystem exchange over the period 2011–2020 and indicated that these changes have already transformed the ecosystem from a CO_2 sink into a source. These results can be used to improve our understanding of the sensitivity of ecosystem respiration to increased warming during the non-growing period.

Plain Language Summary Cold region ecosystems store vast amounts of soil organic carbon (SOC), which upon warming and decomposition can affect the net carbon balance and potentially change these ecosystems to become a source of carbon dioxide (CO_2) to the atmosphere. We have measured year-round CO_2 fluxes over 10 years from an alpine steppe-ecosystem on the Tibetan Plateau. The results show that the region has experienced pronounced warming during the study period and that the resulting near-surface soil warming is a key parameter for explain why the ecosystem over 10 years have changed from being a net sink to become a net source of CO_2 to the atmosphere. Measurements year-round demonstrate that the shift in the CO_2 balance is mainly due to a marked increase in decomposition of SOC during the non-growing-season. Furthermore, observations reveal several high-emission events at the end of the non-growing season and early in the growing season, which have increased in importance during the study period. The results are important to improve our understanding of the sensitivity of cold ecosystem respiration to warming and to highlight the importance of winter processes and emissions events on the annual ecosystem carbon budget.

Key Points:

- Warming of the Tibetan Plateau has consequences for the net carbon balance
- Significant warming has resulted in a net carbon loss from soil respiration
- The steppe-ecosystem has changed from being a sink to a source of CO_2 to the atmosphere

Supporting Information:

Supporting Information may be found in the online version of this article.

Correspondence to:

Q. Wu, A. Chen, and B. Elberling,
qbwu@lzb.ac.cn;
apchen1111@gmail.com;
be@ign.ku.dk

Citation:

Yun, H., Tang, J., D'Imperio, L., Wang, X., Qu, Y., Liu, L., et al. (2022). Warming and increased respiration have transformed an alpine steppe ecosystem on the Tibetan Plateau from a carbon dioxide sink into a source. *Journal of Geophysical Research: Biogeosciences*, *127*, e2021JG006406. https://doi.org/10.1029/2021JG006406

Received 26 MAY 2021
Accepted 22 NOV 2021

Author Contributions:

Conceptualization: Hanbo Yun, Qingbai Wu, Anping Chen
Data curation: Hanbo Yun, Jing Tang, Ludovica D'Imperio, Qingbai Wu
Formal analysis: Hanbo Yun, Jing Tang, Deliang Chen, Bo Elberling
Funding acquisition: Qingbai Wu, Bo Elberling
Investigation: Hanbo Yun, Qingbai Wu, Anping Chen
Methodology: Hanbo Yun, Qingbai Wu, Anping Chen, Bo Elberling
Project Administration: Qingbai Wu, Anping Chen, Bo Elberling

Resources: Hanbo Yun, Ludovica D'Imperio, Xiaobo Wang, Yang Qu, Licheng Liu, Qianlai Zhuang, Wenxin Zhang, Qingbai Wu, Anping Chen, Bo Elberling
Software: Hanbo Yun
Supervision: Hanbo Yun, Ludovica D'Imperio, Wenxin Zhang, Qingbai Wu, Anping Chen, Bo Elberling
Validation: Hanbo Yun
Visualization: Hanbo Yun, Bo Elberling
Writing – original draft: Hanbo Yun
Writing – review & editing: Jing Tang, Ludovica D'Imperio, Xiaobo Wang, Yang Qu, Licheng Liu, Qianlai Zhuang, Wenxin Zhang, Qingbai Wu, Anping Chen, Qing Zhu, Deliang Chen, Bo Elberling

1. Introduction

The Northern Hemisphere permafrost region stores carbon (C) as soil organic C equal to roughly twice the amount present in the atmosphere (Hugelius et al., 2013). The net ecosystem exchange of carbon dioxide (CO_2) depends on the balance of decomposition of soil C reserves and the fixation of atmospheric CO_2 by vegetation (Davidson & Janssens, 2006; Euskirchen et al., 2017). Warming of the active layer (AL, defined as the portion of the soil profiles thawing each summer) and thawing of previously frozen soils can stimulate soil organic matter decomposition and thus increase ecosystem heterotrophic respiration, leading to a positive feedback in terms of atmospheric CO_2 concentration (Elberling et al., 2013; Plaza et al., 2019; Schuur et al., 2009). In contrast, wetter conditions and changes in oxygen availability in the soil may lead to reduced respiration rates and consequently increased protection of the soil C reserves (Elberling et al., 2013; Schuur et al., 2021). Moreover, the combination of warming, increasing soil moisture and higher atmospheric CO_2 concentrations can also increase net primary production (NPP) through enhancing plant productivity (Epstein et al., 2013) and change the plant community composition (Bjorkman et al., 2018; Zhu et al., 2016).

There is still no consensus among observational and modelling studies with respect to permafrost-affected ecosystems functioning as a net CO_2 sink or source (Celis et al., 2017; Zhang, Zhang, et al., 2018). Most studies agree that tundra ecosystems over the past 100–1000 years have functioned as net CO_2 sink areas (Min et al., 2021; Prik et al., 2017). However, site-specific studies have shown that tundra can function as either a net CO_2 source or sink under recent climate warming (Lupascu et al., 2014; Oechel et al., 2000; Schuur et al., 2015; Wickland et al., 2020). A recent review demonstrated that across 148 terrestrial high-latitude sites, the net ecosystem exchange (NEE) in the period 1990–2015 indicated that the region was on average an annual CO_2 sink although uncertainty remains high (Vikkala et al., 2021). All of these studies mainly focus on the Arctic (high-latitude) permafrost region and are rarely extended to high altitudes (Ding et al., 2016). Therefore, it remains unclear whether the underlying mechanisms and processes found at high latitudes also apply to high-altitude regions (Yun et al., 2018).

The Tibetan Plateau has the largest extent of high-altitude permafrost in the world (Chen et al., 2015) and has experienced pronounced warming, wetting, and permafrost degradation over recent decades (Yao et al., 2019). The environmental changes and alteration of ecosystem C processes could lead to changes in CO_2 flux (Wei et al., 2021; Yun et al., 2018). This study examined the temporal variations and trends of ecosystem CO_2 exchange by combining plot-scale (<1 m^2 by automatic chambers) and landscape (>10,000 m^2 by EC) CO_2 measurement data at an experimental site in the Tibetan Plateau. The site is known to be a C sink area (Piao et al., 2019) but is currently subject to marked warming (Wu et al., 2015). The present study is based on the following hypotheses: (1) ecosystem respiration will be controlled by both warming and changes in soil moisture. Therefore, an increase in ecosystem respiration is expected during warm periods if changes in soil moisture are not limiting the availability of water (too dry) or oxygen (too wet); (2) warming and changes in soil moisture will similarly regulate plant growth and thereby influence NEE; (3) the net effect of plant growth and respiration on NEE is expected to vary from year to year, and only measurements made across multiple years will allow a sensitivity analysis of NEE with respect to environmental factors as well as robust measures of current CO_2 sink/source capacity. Answering these questions will help us to understand how alpine steppe ecosystems respond to climate-induced warming on the Tibetan Plateau and ultimately to predict the potential changes in ecosystem carbon balance.

2. Methods

2.1. Site Descriptions and Setup

This study was conducted near the Beilu'He research station located in a representative permafrost region (Niu et al., 2019) on the Tibetan Plateau (34°09′06″N, 92°02′57″E; Figure S1), with an altitude of about 4670 m. From 2010 to 2020, the mean annual temperature varied from −3.1°C to −2.3°C, the mean annual precipitation ranging between 287.4 and 440.8 mm, and the Palmer aridity index ranging from 0.4 to 0.6 (Ding et al., 2017). The dominant vegetation type is alpine steppe with the following corresponding dominant species: *Carex moorcroftii Falc. ex Boott, Kobresia tibetica Maxim androsace tanggulashanensis*, and *Rhodiola tibetica*. The mean plant height was 13.7 ± 4.6 cm, and the mean rooting depth was 21.2 ± 5.4 cm. Two dwarf deciduous shrubs *(Potentilla parvifolia* Fisch. *ex. Lehm*. and *Myricaria prostrata Hook. f. et Thoms. ex Benth)* were first identified in 2013 (Yun et al., 2018). The aboveground and belowground (0–100 cm) biomasses ranging from 108.2 ± 30.8

to 124.5 ± 42.5 g m^{-2} and 2427.0 ± 61.9 to 2710.3 ± 47.1 g m^{-2}, respectively. The main soil type is Inceptisol (Soil Taxonomy; USDA, 1999) or Cambisol (World Reference Base for Soil Resources; FAO. IUSS Working Group WRB, 2014). The main body of the permafrost was formed during the late Pleistocene Last Glaciation Maximum (26,500–19,000 years BP; Zhou et al., 2001) but experienced extensive degradation after the warming period during the Holocene (8500–4000 years BP; Jin et al., 2007). Subsequently, new permafrost formed during the Neoglaciation period (4000–1000 years BP; Jin et al., 2007). Currently, the average active layer thickness is ∼1.9 m (Cheng et al., 2019) and increased at a rate of >1.3 cm yr^{-1} from 1995 to 2007 (Wu & Zhang, 2010).

The EC-based CO_2 fluxes were measured from July 2010 to December 2020. The CO_2 fluxes were simultaneously measured at the plot level (100 × 100 cm^2) using automatic chambers, with the first measurement beginning in May 2012. The automatic chamber plots were located just outside the tower fetch, within the EC footprint area with a similar vegetation community and similar soil and climatic conditions.

2.2. Environmental Monitoring

A Campbell weather station (Campbell, Salt Lake City, USA) was used to monitor the environmental parameters and was installed on a 10 m mast and placed about 1.3 km away from the EC tower. Air temperature, air pressure, and air humidity were measured 3 m above the ground, with precisions of ±0.1°C and 0.1%, respectively (HMP45 C, Vaisala Inc., Finland). Incident and net radiation were monitored by a four-component net radiometer (Rn; CNR-1, Netherlands), mounted on the tower 3 m above the soil surface. The wind direction and wind speed were measured 3 m above the ground with a propeller anemometer (P2546, Campbell, Salt Lake City, USA). Half-hourly interval data were automatically recorded with a data logger (CR3000, Campbell, Salt Lake City, USA). Soil heat flux was monitored by two precalibrating soil heat flux sensors (HFP01, Netherlands) and inserted 5 and 15 cm below the ground. Air pressure was measured by a CS100 barometer (CS100, Campbell, Salt Lake City, USA).

The temperature of the permafrost was continuously monitored using two permafrost boreholes by constantan-copper thermocouples at 50 cm intervals to a total depth of 50 and 100 m and adjacent to the EC tower. Soil temperature and soil water tensions were monitored near the micrometeorological tower with a group of pF-meter sensors (soil temperature and soil water tension precision were ±0.25°C and ±0.05, respectively; GEO-Precision, Germany), at 10 cm resolution in the upper 100 and 50 cm^2 intervals to a depth of 550 cm. An additional 10 cm resolution was obtained near the former permafrost table from 150 to 300 cm depth. Precipitation was monitored with a TE525MM rain gauge (precision is ±0.1 mm; Texas Electronics Inc., USA). All data were measured every 5 min and averaged at half-hour intervals, recorded with data logger CR3000 (Campbell, Salt Lake City, USA). Soil temperature data from two different sensors were calibrated by the Meteorological Data Service Center, the State Key Laboratory of Frozen Soil Engineering, China.

Soil physical and chemical properties of 240 soil and sediment samples collected within 100 m of the EC tower were analyzed at the State Key Laboratory of Frozen Soil Engineering, China. Topsoil samples (0–100 cm) were sampled using a soil corer (5 cm diameter) at 10 cm intervals. For samples below 100 cm we used a motorized drill to collect samples at 50-cm intervals to a depth of 500 cm in the middle of September every year from 2008 to 2020. The samples were collected using a stainless-steel ring cutter with three replicates. The permafrost table was determined by the ice content of the core sampling. All samples were marked and sealed in a 100-ml steel aluminum box, weighed, frozen at −15°C, and brought back to the laboratory. The SOC of the air-dried soil samples was analyzed using the wet combustion method, Walkley-Black modified acid dichromate digestion, $FeSO_4$ titration and an automatic titrator. TN was measured by an elemental analyzer (Vario EL Three, Elementar, Germany). The soil C:N ratio was then calculated as the quotient of the SOC and the TN concentration. The soil pH level was determined by amperometry (DJS-1C, Leizi, Shanghai, China).

2.3. Carbon Dioxide Flux Measurements

Net ecosystem exchange (NEE) was monitored by the automatic chambers at the plot scale and by the eddy covariance tower (EC) at the landscape scale. Here, the positive (+) and negative (−) values of the CO_2 fluxes represent net ecosystem carbon emission and net carbon uptake, respectively.

2.3.1. Automatic Chamber Setup

The ecosystem NEE (μmol C m^{-2} s^{-1}) and respiration (R_{eco}, μmol C m^{-2} s^{-1}) were measured using three translucent chambers and three dark chambers equipped with an automated CO_2 flux chamber system (Li-Cor 8100 extended by Li-Cor 8150, USA) at six different locations. From 1st May to 30th September, the chamber was set to measure at a rate of 5 min hr^{-1} and from 1st October to 30th April, it was set to measure at 10 min hr^{-1}. Air temperature, air pressure, moisture, and CO_2 concentrations within the chamber and CO_2 concentrations in the atmosphere were recorded using a Li-Cor 8100. The chamber NEE data were expressed as μmol CO_2 m^{-2} s^{-1} using the plot-specific chamber air pressure, air temperatures, and chamber volume. The flux data were then screened for any equipment failure, power outage and/or any unsuitable environmental conditions producing erratic fluxes (such as wind speeds exceeding 10 m s^{-1}). After screening, about 83% of total flux measurements were used for further analysis. A more detailed description of the data processing can be found in Mauritz et al. (2017).

2.3.2. Eddy Covariance Setup

The NEE was also directly measured by the EC tower. The EC system was mounted at a 3 m height, including a sonic anemometer (CSAT3, Campbell, Salt Lake City, USA) and an open path infrared gas analyzer (LI-7500A, LI-COR Biosciences, USA). In July 2017, the open path infrared gas analyzer was updated to LI-7500RS (LI-COR Biosciences, USA). The data for wind, CO_2, water vapor and air temperature were recorded by the LI-COR 7550 analyzer (LI-COR Biosciences, USA). The measurements with the LI-7500A and LI-7500RS analyzers, including CO_2, water vapor and dew point, were calibrated by the China Land-Atmosphere Coordinated Observation System. Fluxes were computed from the covariance of CO_2 and vertical wind speed using Eddypro 6.2.0 (Li-Cor Biosciences, USA) and reported as an average over 30-min intervals.

The tilt correction algorithm was adopted for the correction of wind resulting from any sonic anemometer misalignment in terms of local wind streamlines (Wilczak et al., 2001). Here, the fluxes were corrected using the wind axis double ration method (Aubinet et al., 1999) and then corrected by time lag with covariance maximization, air density, frequency loss, and sensor separation according to Burba et al. (2008), with statistical testing following Vickers and Mahrt (1997), including accepted spikes at a threshold of ≤1% and if spikes >1%, they were excluded and replaced with new data by linear interpolation. The plausible ranges of wind were five standard deviations (SD), whereas those for water (H_2O) and CO_2 were 3.5 SD. Post-field data processing included data (1) that contained any missing data points, (2) where friction velocity (U*) was smaller than 0.10 m s^{-1} (Goulden et al., 1996), or (3) where standard deviation of the orthogonal wind components was greater than one sigma from the mean. In contrast to LI-7500, the two analyzers used here, LI-7500 A/RS, did not need any corrections to account for additional instrument-related sensible heat flux according to the instruction manual for Eddypro 9.0.

Data QA/QC flagging was based on developed turbulence tests and steady states, giving three levels of data quality, where 0 indicated high (58% in this study), 1 indicated intermediate (19%), and 2 indicated poor quality data (18%, not including missing data, which accounted for 5% of the total data), which were discarded when calculating the yearly and seasonal C budgets (Belshe et al., 2012; Yun et al., 2018). The footprint of the EC tower ranging from 115 to 172 m, estimated based on the method of Kljun et al. (2015), which covered a similar vegetation and permafrost state. The surface energy balance ratio (EBR) was calculated based on the method of Wilson et al. (2002). The mean EBR value was about 0.68, which is within the range given by the global FLUXNET (from 0.34 to 1.69; Wilson et al., 2002).

2.4. Gap Filling and Budget Calculations

Based on growing degree days (GDD) and phenology recorded from 1975 to 2020, Beilu'He Station's growing season starts around 10th May and ends on 30th September. Thus, the subsequent non-growing season starts around 1st October and ends on 9th May. In order to enable comparison with other studies, the growing season is in the following defined as the period between 1st May and 30th September while 1st October to 30th April is considered the non-growing season.

Missing data from the EC tower due to harsh weather conditions and power issues represent 23% of the data gathered over the entire study period, which were subsequently filled using growing season- and non-growing season-specific models (Tovi Data Analysis software, Li-Cor Biosciences, USA). For auto-chambers, there was

a 17% data gap for CO_2 fluxes over the whole period. All CO_2 fluxes were measured and gap-filled at 30-min intervals and then aggregated to daily, seasonal and annual sums.

Uncertainties regarding the gap-filled EC data were assessed by bootstrapping to determine the difference between measured mean value and standard deviation (SD). Correlation regression studies were done to determine the difference between the gap-filled and measured EC data; the significance level was $P < 0.05$. In each category, artificial data sets were created by adding predicted model values to randomly drawn and replaced residuals, and models were refit in order to gap-fill data. The 95% confidence interval was obtained from 1000 complete flux time series for seasonal cumulative fluxes. Auto-chamber uncertainties were based on SD of replicate plot measurements, $n = 6$.

2.4.1. Growing Season Gap Filling

In daytime, the gaps in EC-based NEE data were filled using the hyperbolic light response equation when the PAR values were higher than 10 μmol m^{-2} s^{-1} (Thornley & Johnson, 1990). For the automatic chambers, hyperbolic light response curves were generated for each individual plot and were then used to gap-fill the NEE data on a monthly basis. For night-time NEE, the gaps (R_{eco}, PAR <10 μmol m^{-2} s^{-1}) were filled using the exponential temperature response curves together with the soil temperature of 10 cm for the automatic chamber and the air temperature 3 m from the EC system. The Q10 value used for temperature responses of ecosystem respiration was 4.3 (Chen et al., 2016), derived from night-time NEE temperature responses. The correlation regression fit result show that the $p < 0.01$, $R^2 = 0.84$, RMSE = 3.37 (root mean square error) between mean value of model gap-filled data and EC measured data, whereas the $p < 0.01$, $R^2 = 0.91$, RMSE = 1.57 for the automatic chamber. The gross ecosystem primary productivity (GPP) was estimated by subtracting R_{eco} from NEE.

2.4.2. Non-Growing Season Gap-Filling

Non-growing season gap-filling and cumulative CO_2 flux assessment were divided into autumn (October), winter (November–January), and spring (February–April). This study accounts for GPP in the autumn (October) and spring (February to April). Potential impacts from the lengthened growing season on the measured CO_2 fluxes have previously been discussed (Ueyama et al., 2014; Zhu et al., 2020).

In the autumn (October) and spring (February to April), for the chamber, NEE and R_{eco} were fitted using response curves to weekly light and temperature. R_{eco} in spring (February–April) was estimated using the winter model for both automatic chambers and EC, as soils were frozen. The NEE for spring (February to April) was analyzed based on the sum of GPP and R_{eco} (Webb et al., 2016). For the EC, autumn (October) and spring (February to April) NEE were computed weekly where GPP could be detected. R_{eco} fluxes in winter (November to January) were gap-filled based on the exponential relationship between NEE and soil temperature of 0–30 cm. The correlation regression fit result show that the $p < 0.01$, $R^2 = 0.87$, RMSE = 2.65 between mean value of model gap-filled data and EC measured data, whereas the $p < 0.01$, $R^2 = 0.94$, RMSE = 1.18 for the automatic chamber.

2.5. Data Analysis

The differences at annual, growing season and non-growing season time scale NEE/GPP/Reco were used bootstrapped to calculate the mean (95% confidence interval) to test for significant difference. For the auto-chamber, similar seasonal differences have been analyzed using a *post-hoc Tukey test* and ANOVA. Bootstrapping, a *post-hoc Tukey* test, and ANOVA were implemented using R 3.6.3 (R Development Core team, 2020) and the significant level of alpha tested based on an acceptable level of 0.05. Correlation analyses were conducted to examine the relationships between NEE and environmental factors, the thickness of the active layer and monthly soil properties during the growing season. Soil properties included soil organic carbon (SOC) content, carbon-to-nitrogen ratio (C/N), and soil pH. All of the above data of the Beilu'He station during the observation period were obtained from the State Key Laboratory of Frozen Soil Engineering and the measurement of the data was detailed in Yun et al. (2018) as well as the NEE of the non-growing season with the above-mentioned variables. All data are presented as mean values with standard deviations (SD), and the confidence interval is 95%.

Structural equation modeling (SEM) was conducted to quantify the direct and indirect processes in regulating NEE at different seasonal intervals (annual, growing season and non-growing season). SEM is a multivariate statistical analysis technique and in the model, the hypothetical pathways of influence between different variables can be designed and tested based on our understanding of process interactions (Miao et al., 2009). This technique

Table 1
Environmental Variables Measured at the Site During Growing Season (Grow Seas.), Non-Growing Season (N-Grow. Seas.), and the Reference Period Between 1st March and 15th June Used as a Proxy for the High Carbon Dioxide Emissions at the End of the Non-Growing Season and at the Start of the Growing Season

	2010–2020			Long-term (1975–2020)		
Environmental variables	Grow. Seas.	N-Grow. Seas.	1st March to 15th June	Grow. Seas.	N-Grow. Seas.	1st March to 15th June
Tair (°C)	4.0 ± 3.2	−8.9 ± 2.9	−3.5 ± 3.3	3.9 ± 1.6	−10.2 ± 5.1	−3.7 ± 2.2
Rainfall (mm)	35.0 ± 26.0	23.0 ± 14.0	67.0 ± 18.0	316.0 ± 20.0	21.0 ± 11.0	40.0 ± 16.0
Wind Speed (m s^{-1})	3.5 ± 2.7	5.1 ± 1.9	4.6 ± 1.8	3.3 ± 2.7	4.6 ± 4.1	4.2 ± 3.8
Tsoil (°C)	4.3 ± 3.0	−4.4 ± 3.8	−2.3 ± 2.9	3.7 ± 3.2	−4.6 ± 3.6	−2.5 ± 2.1
SWC (%)	14.4 ± 1.8	-	11.6 ± 2.0	15.0 ± 2.7	-	9.2 ± 7.3
TSF (cm)	7.7 ± 3.4	65.5 ± 12.4	53.6 ± 18.3	6.5 ± 5.9	35.1 ± 22.6	30.9 ± 16.3
SCD (d)	11.0 ± 10.0	47.0 ± 16.0	39.0 ± 15.0	13.0 ± 11.0	24.0 ± 13.0	18.0 ± 11.0
ALT (cm)	185.0 ± 17.0	-	36.0	132.0 ± 38.0	-	32.0

Note. Tair, air temperature at 3 m (°C); Rainfall, mm. The non-growing season rainfall does not include snow because the rainfall was measured by a rain gauge only. Data for the total snowfall and snow cover days were obtained from the Wudao-Liang meteorology service station, located 52 km away from the EC tower; Tsoil: soil temperature at 0–30 cm (°C); SWC, soil water content at 0–30 cm (%); TSF, total snowfall (cm); SCD, snow cover days (d); ALT, the thickness of the active layer (cm); Grow. Seas., growing season, from 1st May to 30th September; N-Grow. Seas, non-growing season, from 1st October to the next 30th April. Data presented are given as means ± SD. The Values are Reported for the Decade 2010–2020 and the Long-Term 1975–2020.

goes beyond traditional multivariate techniques by integrating knowledge-based interactions among different variables (Grace, 2006).

To investigate seasonal differences in the underlying mechanisms that drive the interannual variations of NEE, two SEMs were constructed for the growing season and non-growing season separately. Model construction and model optimization were carried out to obtain the final SEM. In this study, driving variables were only included if they were significantly correlated with the response variable in the model, which was done through the correlation analysis between different driving variables and the response variable (NEE; Table S1). Subsequently, different pathways between these driving variables and the response variable were designed. The CO_2 flux uptake or release in the permafrost-affected ecosystem and permafrost warming (i.e., the thickness of the active layer) were assumed to play direct roles in the NEE process. Furthermore, environmental factors (i.e., soil temperature and soil water content, air temperature, vapor pressure deficit, net radiation) can have a direct effect on NEE, as we presumed that soil properties can directly/indirectly impact NEE. Given that GPP and R_{eco} were modeled by the NEE observation, the GPP and R_{eco} were not used in the SEM calculations.

The model was iteratively optimized based on the measurement data over the same periods, following Colman and Schimel (2013), by gradually removing pathways with $P > 0.05$. The chi-square statistic (χ^2) and the root-mean-square error of approximation (RMSEA) were used to assess the overall goodness of each model (Asparouhov et al., 2018; Grace, 2006). A normal distribution test was performed using the Kolmogorov–Smirnov method for all the data, and the unnormal distributed data were transformed to normal using a logarithmic function. SEM and related statistical analyses were performed using the software R version 3.6.3 with the "sem" and "stats" packages.

3. Results

3.1. Environmental Conditions

Annual mean air temperature measured at 3 m was −3.5 ± 1.7°C (result ± SD) for the measurement period (2010–2020), which is significantly higher than that for the period of 1975–2020 (hereafter described as "long-term," −4.2°C ± 2.2°C) for this region (Table 1). Air temperatures during the growing seasons were of similar magnitude to the long-term mean for this region (4.0 ± 1.6 vs. 3.9 ± 3.2°C). However, for the non-growing season, air temperature of the period 2010–2020 was significantly higher than the long-term mean. Mean air temperature warming was significant both for the non-growing season and annual in the period 2010–2020 (0.18°C and 0.13°C over 10 years, respectively), whereas the growing season showed no significant change (0.1°C per 10 years; $P = 0.053$).

From 2010 to 2020, the mean annual precipitation (snowfall and rainfall) was 395 mm, which ranging from 276 mm in 2014 to 385 mm in 2019, and was higher than the long-term average (377 mm, $P = 0.05$). The relative length of the growing and non-growing seasons (2010–2020) was not significantly different from that of the long-term average, but the sum snowfall and total numbers of days with snow cover increased significantly from 2010 to 2020 (Figure S2) and were also higher than the long-term average (53.6 ± 18.3 vs. 30.9 ± 16.3 cm for sum snowfall and 41.0 ± 15.0 vs. 18.0 ± 11.0 days for snow cover time, respectively; Table 1). The mean annual soil temperature for 0–30 cm was −0.8°C in the period 2010–2020, higher than the long-term average of −1.2°C. The mean soil water content for 0–30 cm during the growing season was 11.3% from 2010 to 2020, which was not significantly different from the long-term average (10.8%). The mean active layer thickness (ALT) on Beilu'He was 185 ± 17 cm and significantly increased by a rate of 3.5 cm yr^{-1} in the period 2010–2020, resulting in a considerably deeper ALT than the long-term average (mean ALT was 132.0 ± 38.0 cm).

3.2. Temporal Dynamics of Ecosystem Carbon Dioxide Flux

During 2011–2020, the mean annual ecosystem carbon exchange (NEE) rate measured by EC was 1.4 ± 15.5 g C m^{-2} yr^{-1} (ranging from −28.1 ± 20.0 g C m^{-2} yr^{-1} of 2012 to 18.6 ± 17.59 g C m^{-2} yr^{-1} of 2017), lower than the value of 4.9 ± 13.5 g C m^{-2} yr^{-1} which was measured by the automatic chamber for the period 2013–2020 (ranging from −10.8 ± 17.0 g C m^{-2} yr^{-1} for 2014 to 21.9 ± 13.8 g C m^{-2} yr^{-1} for 2017) (Figures 1a and 1b). The ANOVA results indicate that the NEE rates measured by both EC and the automatic chamber significantly increased during the study period ($p < 0.01$). During the growing season (first May to 30th September), the ecosystem was a consistent CO_2 sink, while for the non-growing season (1st October to 30th April), the ecosystem was a consistent CO_2 source over the entire study period. Specifically, the mean NEE rates of the growing season were −34.7 ± 11.4 g C m^{-2} yr^{-1} (ranging from −50.9 ± 14.8 in 2013 to −21.0 ± 24.6 g C m^{-2} yr^{-1} in 2011) and −39.2 ± 8.4 g C m^{-2} yr^{-1} (ranging from −52.5 ± 18.5 g C m^{-2} yr^{-1} in 2016 to −23.9 ± 12.7 g C m^{-2} yr^{-1} in 2019), measured by EC and the automatic chamber, respectively. For the non-growing season, the mean NEE rate measured by EC was 33.3 ± 6.9 g C m^{-2} yr^{-1}, with a clear increase of about fivefold from 9.3 ± 17.6 g C m^{-2} yr^{-1} of 2011 to 49.5 ± 26.5 g C m^{-2} yr^{-1} of 2020.

Surprisingly, several high CO_2 emission events were noted at the end of the non-growing season and at the start of the growing season, which covered 1st March to 15th June (Figure 2). From 2011 to 2020, the mean CO_2 emission rate of this period was 15.4 g C m^{-2} yr^{-1}, ranging from 14.6 ± 10.7 g C m^{-2} yr^{-1} in 2012 to 35.3 ± 12.1 g C m^{-2} yr^{-1} in 2017. Emissions significantly increased over the period 2011–2020, with an average rate of 22.6 g C m^{-2} $decade^{-1}$ (Figure S3), which accounted for annual emissions of 23.2% and 25.8%, respectively.

Figure 1 indicates that the mean annual R_{eco} based on EC was 81.3 ± 14.1 g C m^{-2} yr^{-1}, slightly lower than that measured by the automatic chamber (84.3 ± 10.3 g C m^{-2} yr^{-1}). The highest annual R_{eco} was found in 2019 for EC, whereas it occurred in 2017 for the automatic chamber method. In addition, the minimum values of R_{eco} occurred in 2013 for both the EC and automatic chamber measurements.

From 2011 to 2020, the annual EC-measured R_{eco} showed a significant increase at a rate of 26.3 g C m^{-2} $decade^{-1}$, ranging from 55.2 ± 13.8 g C m^{-2} yr^{-1} to 100.8 ± 12.6 g C m^{-2} yr^{-1} (the automatic chamber increased at a rate of 32.9 g C m^{-2} $decade^{-1}$, ranging from 67.5 ± 27.6 g C m^{-2} yr^{-1} to 98.0 ± 15.6 g C m^{-2} yr^{-1}). During the growing season, the mean R_{eco} was 36.2 ± 8.2 g C m^{-2} yr^{-1} with EC, which is very similar to the automatic chamber measurement (31.1 ± 7.3 g C m^{-2} yr^{-1}). There were no significant changes in the R_{eco} of the growing period in both the EC and automatic chamber measurements. For the non-growing season, R_{eco} accounted for more than half of the total annual R_{eco} (55.9% for EC and 62.9% for the automatic chamber).

The mean annual GPP was −78.4 ± 8.1 g C m^{-2} yr^{-1} for both the EC and automatic chamber and showed no significant interannual variability ($p > 0.05$; Figure 1). The growing season accounted for 87.6% and 86.1 of the annual GPP for the EC and automatic chamber measurements, respectively. The non-growing season contributed relatively little to the annual GPP (−18.4 ± 12.4 to −0.4 ± 20.7 g C m^{-2} yr^{-1} for the EC and automatic chamber measurements, respectively), and no significant change was found over time with either method.

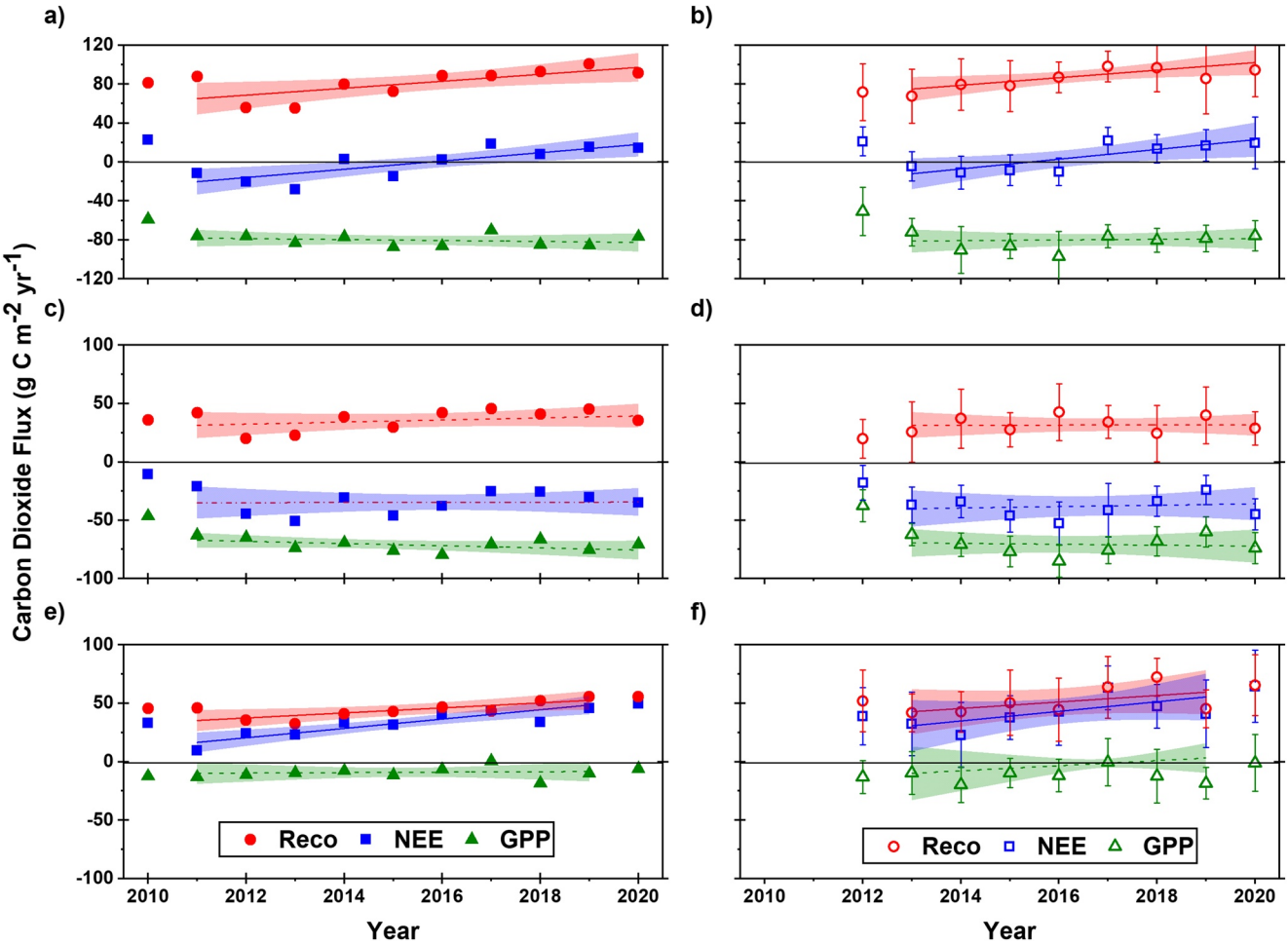

Figure 1. Time series of carbon dioxide (CO_2) flux from an alpine steppe in Beilu'He, northwest Tibetan Plateau using eddy-covariance (left column, solid symbols) and chamber-based (right column, open symbols) approaches. (a) and (b) annual total of CO_2 fluxes, (c) and (d) CO_2 fluxes for the growing season, (e) and (f) fluxes for non-growing season. NEE, net ecosystem exchange (NEE, g C m^{-2} yr^{-1}); R_{eco}, ecosystem respiration (g C m^{-2} yr^{-1}); GPP, gross primary production (g C m^{-2} yr^{-1}). The linear regression of annual total and growing season fluxes was based on the period 2011–2020, as we only had the July measurement for 2010. For fluxes from the non-growing season, the linear regression was based on 2011–2019, because we lacked complete measurements for 2010 and 2020. Solid lines are used to mark significant ($p < 0.05$) changes, whereas dashed lines indicate non-significant changes ($p > 0.05$). Shading illustrates the 95% confidence intervals.

3.3. Drivers of Carbon Dioxide Flux

The Structure equation modeling (SEM) illustrates the direct and indirect links between net ecosystem exchange (NEE), environmental variables and the thickness of the active layer, soil temperatures of 0–30 cm, and soil water content of 0–30 cm (Figure 3). Here, important drivers of NEE in the growing season were identified: active layer warming and soil properties. The SEM model suggests that the active layer warming and soil properties could explain 78% of the NEE variations during the growing season and that active layer warming alone could explain 64% of the NEE in the non-growing season (Figure 3).

4. Discussion

4.1. Ecosystem Carbon Budget for the Alpine Steppe Ecosystem on the Tibetan Plateau

Ten years of year-round carbon dioxide (CO_2) flux measurements in the alpine steppe ecosystem of the Beilu'He region on the Tibetan Plateau show that the site has switched from being a net annual sink (or close to neutral) of CO_2 to a net source of CO_2 to the atmosphere (the shift was from -28.1 ± 20.0 to 21.9 ± 13.8 g C m^{-2} yr^{-1}). The study site is dominated by the following plant species: *C. moorcroftii Falc. ex Boott, K. tibetica Maxim, A. tanggulashanensis,* and *R. tibetica*, which represent an ecosystem type covering approximately 34%

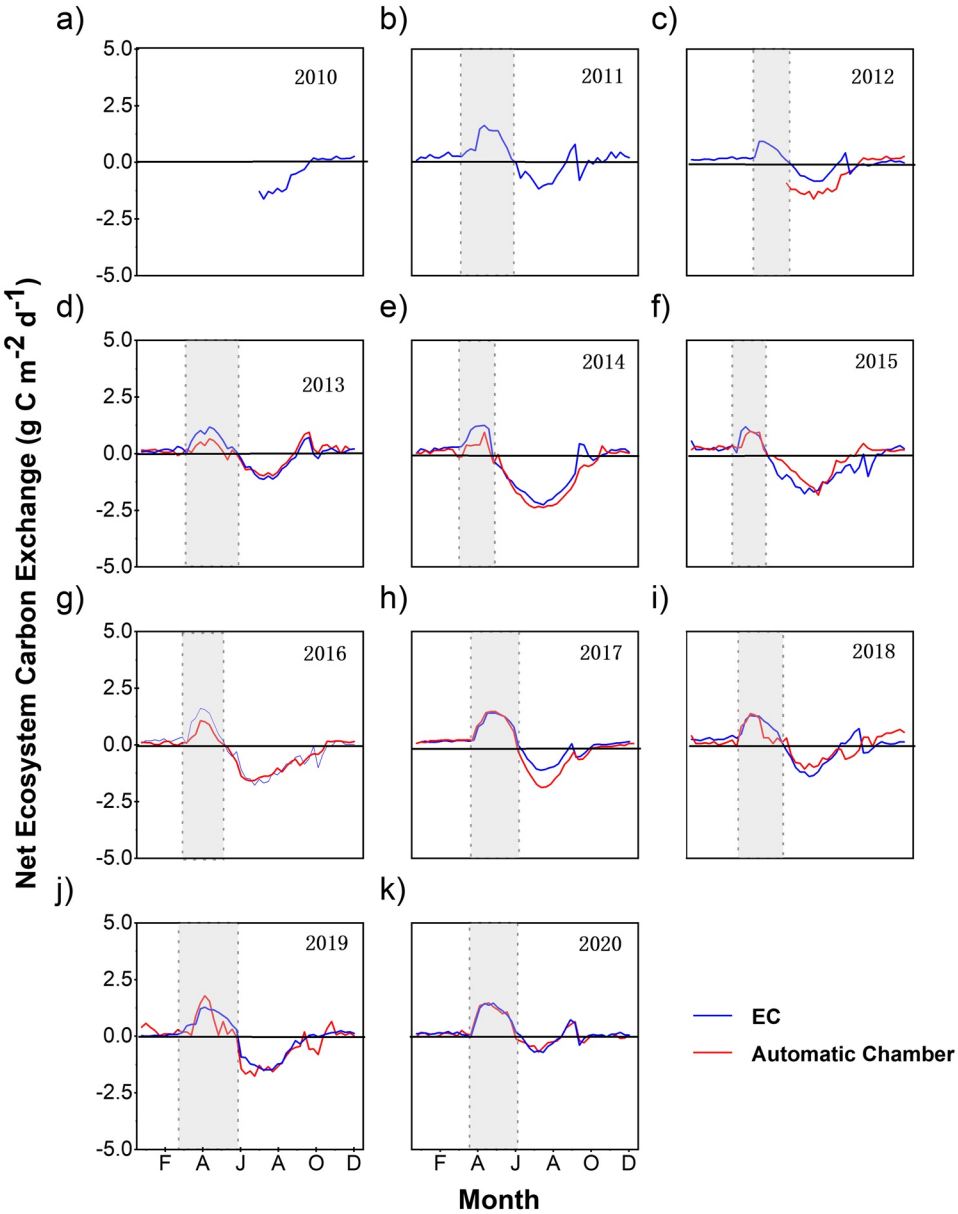

Figure 2. Daily net ecosystem exchange (NEE, g C m^{-2} d^{-1}) measured by the eddy covariance (EC, blue line) and automatic chamber (red line). Gray-shaded areas depict the period with high carbon dioxide (CO_2) emissions from the end of the non-growing season to the early growing season. The start and end time of the CO_2 flux high emission events are marked as gray dotted lines. Here, if the CO_2 emission was five times the mean CO_2 flux of winter for three successive days, it was defined as the start day of the "high emission period." When the CO_2 emission was equal to the mean CO_2 flux of winter for three successive days, it was defined as the end day of the "high emission period".

of the permafrost region on the Tibetan Plateau [the Tibetan Plateau area is 250×10^4 km^2 according to Ding et al., 2016]. Based on the 4.5°C IPCC representative concentration pathway, this type of ecosystem will account for 76% of the Tibetan Plateau in 2100 (Zhang et al., 2015).

Long-term flux measurements carried out in this type of ecosystem are rare (Li et al., 2015; Yun et al., 2018). Most of the reported Tibetan Plateau CO_2 flux data have been collected for wet tundra ecosystems (Liu et al., 2019; Zhang, Zhang, et al., 2018) or seasonal permafrost regions (Li et al., 2016; Niu et al., 2017), in which larger annual rates for GPP and R_{eco} were observed. In this study, annual NEE measurements from both EC and automatic chambers (-1.4 ± 15.5 vs. 4.9 ± 13.5 g C m^{-2} yr^{-1}, respectively) were within the range of the results of other

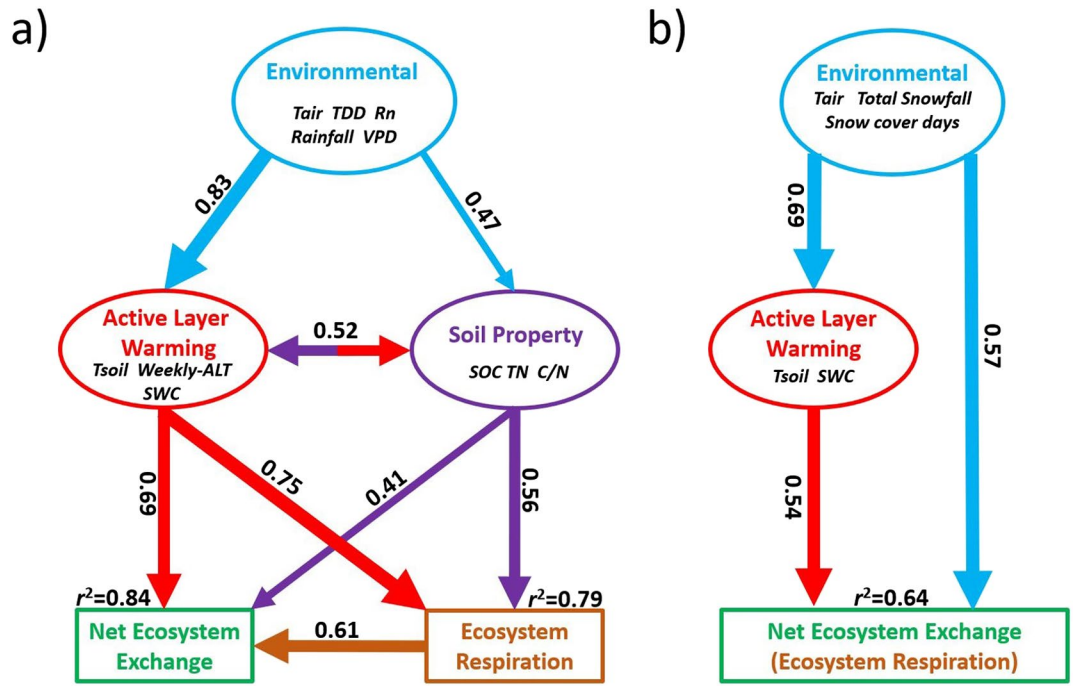

Figure 3. Structural equation modeling (SEM) with considered variables (in colored ellipses) and potential relationships (arrows) for net ecosystem exchange (NEE, green box) over (a) the growing season and (b) the non-growing season using data from EC and the automatic chamber. The double-headed arrows represent the covariance between the two variables. The single-headed arrows indicate the direction of the linkage. The arrow width is proportional to the strength of the path coefficients. The numbers are standardized path coefficients, which reflect the importance of the variables within the model (Colman & Schimel, 2013). "Environmental" includes air temperature at 3 m (T_{air}), thawing degree days (TDD), net radiation (Rn), rainfall, vapor pressure deficit (VPD), total snowfall, and snow cover days. "Active layer warming" includes soil temperature of 0–30 cm (Tsoil), weekly active layer depth (weekly; ALT) and soil water content of 0–30 cm (SWC); "soil property" for 0–30 cm depth includes soil organic carbon (SOC), pH and total nitrogen (TN), and the ratio of SOC to TN concentrations (C/N). The model for the growing season had $\chi^2 = 6.83$ and RMSEA = 0.08, whereas the model for the non-growing season had $\chi^2 = 7.08$ and RMSEA = 0.09.

studies conducted on the Tibetan Plateau or in Arctic tundra upland ecosystems (Kim et al., 2016; Li et al., 2016; Trucco et al., 2012; Zhang, Jansson, et al., 2018).

4.2. Interannual and Seasonal Variations of Carbon Dioxide Fluxes

The trends for interannual variations of the year-round NEE estimated using both EC and automatic chamber measurements revealed that the studied alpine steppe ecosystem has been in transition from being a net CO_2 sink to a net CO_2 source since 2010. This transition has primarily been driven by increasing ecosystem respiration and a corresponding increase in CO_2 emissions during the non-growing season. Our results are in line with a previous meta-data analysis study by McGuire et al. (2012) and Belshe et al. (2013), which suggested that annual CO_2 emissions could exceed CO_2 uptake across the tundra biome, based on 40 years of CO_2 flux data across 32 sites at high latitudes. Our findings also agree with a more recent synthesis study by Natali et al. (2019), based on both process-based models and non-growing season (October–April) CO_2 flux observations across the Pan-Arctic region, which indicates that enhanced soil CO_2 loss as a result of winter warming may offset growing season carbon uptake in the future.

The seasonal pattern of CO_2 fluxes is characterized by considerable CO_2 emissions from the end of the non-growing season to the early growing season (from 1st March to 15th June; Figure 2). The high CO_2 emissions were significantly correlated with total snowfall, snow cover days, and soil water content at 0–30 cm (Figure S4). The start time of high CO_2 emissions was close to the first snow melt event in March (data not shown). The large CO_2 fluxes can be explained by at least two sets of processes: one process related to CO_2 production during winter and trapped CO_2 within the pore space of soils during winter and released upon soil thawing (Elberling &

Brandt, 2003; Raz-Yaseef et al., 2017). The second set of processes is related to potential accelerated microbial activities as well as increased availability of labile C in soils (Pirk et al., 2017). Therefore, the recovery of microbial activity synchronous with the increasing substrate availability could be partly responsible for the relatively large CO_2 emissions (bursts) at the end of the non-growing season and in the early part of the growing season (Liu et al., 2021). Future work is needed to differentiate these two explanations for the Tibetan Plateau study site.

4.3. Key Driver of the Variation of Seasonal Carbon Dioxide Fluxes

In this study, active layer warming was identified as one of the key drivers controlling NEE throughout both the growing and non-growing seasons, which is consistent with the findings of research conducted in Arctic regions (Gerardo et al., 2017; Rodenhizer et al., 2020; Trucco et al., 2012). Increased NEE as a result of active layer warming is associated with increased nutrient availability for both plants and microorganism communities (Hicks Pries et al., 2015) and increased accessibility for microbes to deeper located labile soil carbon pools (Elberling et al., 2010; Koven et al., 2015; Schuur et al., 2007). It is beyond the scope of this study to quantify whether thawing permafrost has directly influenced the increased CO_2 production. But, we conclude that warming and accelerated near-surface SOC turnover alone can explain the observed shift of the ecosystem from being a sink to a source over the studied 10-year period.

From 2010 to 2020, GPP of the growing season as well as the non-growing season showed no significant increase in response to temperature rise, which contrasts with the findings for the Arctic dry tundra that GPP has a higher temperature sensitivity based on open top chamber measurements (Welker et al., 2004) and EC monitors (Ueyama et al., 2014). This suggests that GPP can be affected by changes in vegetation properties, for example, the leaf area index, stomatal conductance (Chen et al., 2021; Grant et al., 2019; Schädel et al., 2018) and other drivers of photosynthesis, for example, air temperature, net solar radiation, soil water content, and even the leaf C/N ratio (Celis et al., 2017; Oechel et al., 2014; Webb et al., 2016). On the Tibetan Plateau, 40 years of monitoring data indicate that significant changes in air temperature and precipitation took place mainly during winter (Yao et al., 2019). Figure 1 suggests that neither the NEE, GPP, nor R_{eco} changed significantly during the growing season over the study period. However, the interannual variations in NEE and R_{eco} and the observations during the non-growing season showed a significant increase, which was mainly explained by the increasing active layer warming over time. The response of increased air temperature during the non-growing season on GPP may however not be representative of other ecosystem types depending on the site-specific hydrological conditions (Welker et al., 2004).

Interestingly, during the growing season, the soil temperature (5.9°C) and soil water content (15%) measured at a 0–30 cm depth interval were comparable to those observed in Arctic heath sites [soil temperature was 5.6°C, and soil water content was 14.5% for 0–30 cm depth; Lund et al., 2012]. However, the mean daily NEE of alpine steppe on the Tibetan Plateau was -1.2 g C m^{-2} d^{-1}, as compared to -0.7 to -0.6 g C m^{-2} d^{-1} at the Arctic heath site. In contrast, NEE measured in this study with EC was almost equal to the NEE measured in a high Arctic semi-desert site on Svalbard [-1.3 g C m^{-2} d^{-1}, measured from 31st July to 11th August; Lüers et al., 2014], with a soil temperature at 0–50 cm depth interval of 6.1°C and SWC <7%. This suggests that soil temperature and SWC may greatly influence the carbon cycle in permafrost-affected ecosystems, but also that regions may differ in terms of carbon sink and source activities despite similarities in the presence of permafrost or short growing seasons. Other environmental factors may control the overall carbon sink/source capacity, such as ALT (Gries et al., 2017), water table depth (Celis et al., 2017), even net radiation (Shen et al., 2015), or soil physical factors, for example, the aggregate protection (Qin et al., 2019).

4.4. Uncertainties and Limitations

In this study, during the winter (November–January), the ground was frozen, and plants were dormant, but a CO_2 uptake was still measurable and documented in data from both EC and the automatic chamber (data not shown) at noon time and low wind speed (<2 m s^{-1}) conditions. It remains unclear what might cause this uptake in winter. Some studies (e.g., Semikhatova et al., 2009; Starr & Oberbauer, 2003) have linked CO_2 uptake in the non-growing season with the photosynthetic activities of evergreen plants and soil crust plants (Starr & Oberbauer, 2003). In this study, we have taken a conservative approach and consider the CO_2 uptake in winter to be negligible. This means there might be slight overestimations of winter CO_2 release.

5. Conclusions

This study summarizes measured CO_2 fluxes in a high alpine steppe site on the northwest Tibetan Plateau (Beilu'He) for the period 2010–2020 using eddy covariance and automatic chamber approaches. During 2010–2020, the study site switched from being a net annual sink of CO_2 or neutral to a net source of CO_2 to the atmosphere. The structural equation model analysis revealed that active layer warming and soil properties were the most important direct drivers of variations in R_{eco} during the growing season (2010–2020). It also showed that active layer warming was the major driver of the R_{eco} changes in the non-growing season linked to changes in snow cover. GPP showed no significant trend corresponding to the warming (mainly during winter), which could be due to a lack of sufficient nutrients despite a warmer climate. Overall, these results imply that changes in NEE reflect several interacting processes regulated by both direct and indirect controls on active layer warming and soil properties. Our hypotheses will now be addressed in turn as follows: (1) ecosystem respiration has increased significantly due to increasing temperatures; mainly during the non-growing season; (2) increased precipitation has not resulted in major changes but has reduced the annual GPP due to a shorter growing season and potential loss of plant-available nutrients; and (3) despite warmer and wetter conditions, increases in plant growth were limited and no changes in GPP were noted during the study period. Thus, this study reveals that the study site and possibly around a third of the Tibetan dry grassland have now switched from being a sink into a source of CO_2 to the atmosphere.

Data Availability Statement

The data generated in this study will be freely available on the Electronic Research Data Archive at the University of Copenhagen (https://sid.erda.dk/sharelink/dgC5Qppkdj, Data ID: dgC5Qppkdj) or the National Cryosphere Desert Data Center, Northwest Institute of Eco-Environment and Resources, Chinese Academy of Sciences (http://www.ncdc.ac.cn/portal/science/list/2).

Acknowledgments
This work was facilitated in part by support provided by the following programs: This study was funded by the Scientific Instrument Developing Project of the Chinese Academy of Sciences, Grant No. YJKYYQ20190012 and the National Natural Science Foundation of China (41501083). We acknowledge Opening Research Foundation of State Key Laboratory of Frozen Soil Engineering, Chinese Academy of Sciences (SKLFSE201812 and SKLFSE201702). Hanbo Yun acknowledges the Strategic Priority Research Program of the Chinese Academy of Sciences (Grant No. XDA19070504) and National Cryosphere Desert Data Center, Northwest Institute of Eco-Environment and Resources, Chinese Academy of Sciences. Qing Zhu was supported by the Reducing Uncertainties in Biogeochemical Interactions through Synthesis and Computation (RUBISCO) Scientific Focus Area, which is sponsored by the Earth and Environmental Systems Modeling (EESM) Program under the Office of Biological and Environmental Research of the US Department of Energy Office of Science. Yang Qu thanks the School of Urban and Regional Science, East China Normal University (Research on Asian Water Tower Changes 13902-412125-20018/005). Wenxin Zhang was supported by the Swedish Research Council VR starting grant 2020-0533 and the Swedish National Space Agency project grant 209/19 and Bo Elberling by the Danish National Research Foundation (CENPERM DNRF100). We would like to thank Yongzhi Liu, Guilong Wu, Ji Chen, and Guojun Liu for their tremendous help in collecting field data over all these years. Thanks to Professor Per-Erik Jansson for providing assistance with the non-growing season data analysis.

References

Asparouhov, T., Hamaker, E. L., & Muthén, B. (2018). Dynamic structural equation models. *Structural Equation Modeling: A Multidisciplinary Journal*, *25*(3), 359–388. https://doi.org/10.1080/10705511.2017.1406803

Aubinet, M., Grelle, A., Ibrom, A., Rannik, Ü., Moncrieff, J., Foken, T., et al. (1999). Estimates of the annual net carbon and water exchange of forests: The EUROFLUX methodology. *Advances in Ecological Research*, *30*, 113–175. https://doi.org/10.1016/S0065-2504(08)60018-5

Belshe, E. F., Schuur, E. A. G., & Bolker, B. M. (2013). Tundra ecosystems observed to be CO_2 sources due to differential amplification of the carbon cycle. *Ecology Letters*, *16*(10), 1307–1315. https://doi.org/10.1111/ele.12164

Belshe, E. F., Schuur, E. A. G., Bolker, B. M., & Bracho, R. (2012). Incorporating spatial heterogeneity created by permafrost thaw into a landscape carbon estimate. *Journal of Geophysical Research: Biogeosciences*, *117*(G1). https://doi.org/10.1029/2011JG001836

Bjorkman, A. D., Myers-Smith, I. H., Elmendorf, S. C., Normand, S., Rüger, N., Beck, P. S., et al. (2018). Plant functional trait change across a warming tundra biome. *Nature*, *562*(7725), 57–62. https://doi.org/10.1038/s41586-018-0563-7

Burba, G. G., McDERMITT, D. K., Grelleanderson, A. D. J., Xu, L., & Xu, L. (2008). Addressing the influence of instrument surface heat exchange on the measurements of CO_2 flux from open-path gas analyzers. *Global Change Biology*, *14*(8), 1854–1876. https://doi.org/10.1111/j.1365-2486.2008.01606.x

Celis, G., Mauritz, M., Bracho, R., Salmon, V. G., Webb, E. E., Hutchings, J., et al. (2017). Tundra is a consistent source of CO_2 at a site with progressive permafrost thaw during 6 years of chamber and eddy covariance measurements. *Journal of Geophysical Research: Biogeosciences*, *122*(6), 1471–1485. https://doi.org/10.1002/2016JG003671

Cheng, G., Zhao, L., Li, R., Wu, X., Sheng, Y., Hu, G., et al. (2019). Characteristic, changes and impacts of permafrost on Qinghai-Tibet Plateau. *Chinese Science Bulletin*, *64*(27), 2783–2795. https://doi.org/10.1360/TB-2019-0191

Chen, A., Mao, J., Ricciuto, D., Xiao, J., Frankenberg, C., Li, X., et al. (2021). Moisture availability mediates the relationship between terrestrial gross primary production and solar-induced chlorophyll fluorescence: Insights from global-scale variations. *Global Change Biology*, *27*(6), 1144–1156. https://doi.org/10.1111/gcb.15373

Chen, D., Xu, B., Yao, T., Guo, Z., Cui, P., Chen, F., et al. (2015). Assessment of past, present and future environmental changes on the Tibetan Plateau. *Chinese Science Bulletin*, *60*(32), 3025–3035. https://doi.org/10.1360/N972014-01370

Chen, L., Liang, J., Qin, S., Liu, L. I., Fang, K., Xu, Y., et al. (2016). Determinants of carbon release from the active layer and permafrost deposits on the Tibetan Plateau. *Nature Communications*, *7*(1), 1–12. https://doi.org/10.1038/ncomms13046

Colman, B. P., & Schimel, J. P. (2013). Drivers of microbial respiration and net N mineralization at the continental scale. *Soil Biology and Biochemistry*, *60*, 65–76. https://doi.org/10.1016/j.soilbio.2013.01.003

Davidson, E. A., & Janssens, I. A. (2006). Temperature sensitivity of soil carbon decomposition and feedbacks to climate change. *Nature*, *440*(7081), 165–173. https://doi.org/10.1038/nature04514

Ding, J., Chen, L., Ji, C., Hugelius, G., Li, Y., Liu, L., et al. (2017). Decadal soil carbon accumulation across Tibetan permafrost regions. *Nature Geoscience*, *10*(6), 420–424. https://doi.org/10.1038/ngeo2945

Ding, J., Li, F., Yang, G., Chen, L., Zhang, B., Liu, L., et al. (2016). The permafrost carbon inventory on the Tibetan Plateau: A new evaluation using deep sediment cores. *Global Change Biology*, *22*(8), 2688–2701. https://doi.org/10.1111/gcb.13257

Elberling, B., & Brandt, K. K. (2003). Uncoupling of microbial CO_2 production and release in frozen soil and its implications for field studies of arctic C cycling. *Soil Biology and Biochemistry*, *35*(2), 263–272. https://doi.org/10.1016/S0038-0717(02)00258-4

Elberling, B., Christiansen, H. H., & Hansen, B. U. (2010). High nitrous oxide production from thawing permafrost. *Nature Geoscience*, *3*(5), 332–335. https://doi.org/10.1038/ngeo803

Elberling, B., Michelsen, A., Schädel, C., Schuur, E. A., Christiansen, H. H., Berg, L., et al. (2013). Long-term CO_2 production following permafrost thaw. *Nature Climate Change*, *3*(10), 890–894. https://doi.org/10.1038/nclimate1955

Epstein, H. E., Myers-Smith, I., & Walker, D. A. (2013). Recent dynamics of arctic and sub-arctic vegetation. *Environmental Research Letters*, *8*(1), 015040. https://doi.org/10.1088/1748-9326/8/1/015040

Euskirchen, E. S., Bret-Harte, M. S., Shaver, G. R., Edgar, C. W., & Romanovsky, V. E. (2017). Long-term release of carbon dioxide from arctic tundra ecosystems in Alaska. *Ecosystems*, *20*(5), 960–974. https://doi.org/10.1007/s10021-016-0085-9

FAO. (2014). *IUSS working group WRB. World reference base for soil resources 2014, International soil classification system for naming soils and creating legends for soil maps*. World Soil Resources Reports No. 106.

Gerardo-Nieto, O., Astorga-España, M. S., Mansilla, A., & Thalasso, F. (2017). Initial report on methane and carbon dioxide emission dynamics from sub-Antarctic freshwater ecosystems: A seasonal study of a lake and a reservoir. The *Science of the Total Environment*, *593*, 144–154. https://doi.org/10.1016/j.scitotenv.2017.02.144

Goulden, M. L., Munger, J. W., Fan, S. M., Daube, B. C., & Wofsy, S. C. (1996). Measurements of carbon sequestration by long-term eddy covariance: Methods and a critical evaluation of accuracy. *Global Change Biology*, *2*(3), 169–182. https://doi.org/10.1111/j.1365-2486.1996.tb00070.x

Grace, J. B. (2006). *Structural equation modeling and natural systems*. Cambridge University Press.

Grant, R. F., Mekonnen, Z. A., & Riley, W. J. (2019). Modeling climate change impacts on an Arctic polygonal tundra: 1. Rates of permafrost thaw depend on changes in vegetation and drainage. *Journal of Geophysical Research: Biogeosciences*, *124*(5), 1308–1322. https://doi.org/10.1029/2018JG004644

Gries, P., Wagner, J., Kandolf, L., Henkner, J., Kühn, P., Scholten, T., & Schmidt, K. (2017). Investigations on soil organic carbon stocks and active layer thickness in West Greenland. *EGU General Assembly Conference Abstracts* (p. 1304).

Hicks Pries, C. E., van Logtestijn, R. S., Schuur, E. A., Natali, S. M., Cornelissen, J. H., Aerts, R., & Dorrepaal, E. (2015). Decadal warming causes a consistent and persistent shift from heterotrophic to autotrophic respiration in contrasting permafrost ecosystems. *Global Change Biology*, *21*(12), 4508–4519. https://doi.org/10.1111/gcb.13032

Hugelius, G., Bockheim, J. G., Camill, P., Elberling, B., Grosse, G., Harden, J. W., et al. (2013). A new data set for estimating organic carbon storage to 3 m depth in soils of the northern circumpolar permafrost region. *Earth System Science Data*, *5*(2), 393–402. https://doi.org/10.5194/essd-5-393-2013

Jin, H., Yu, Q., Lü, L., Guo, D., He, R., Yu, S., et al. (2007). Degradation of permafrost in the Xing'anling Mountains, Northeastern China. *Permafrost and Periglacial Processes*, *18*(3), 245–258. https://doi.org/10.1002/ppp.589

Kim, Y., Park, S. J., Lee, B. Y., & Risk, D. (2016). Continuous measurement of soil carbon efflux with Forced Diffusion (FD) chambers in a tundra ecosystem of Alaska. The *Science of the Total Environment*, *566*, 175–184. https://doi.org/10.1016/j.scitotenv.2016.05.052

Kljun, N., Calanca, P., Rotach, M. W., & Schmid, H. P. (2015). A simple two-dimensional parameterisation for Flux Footprint Prediction (FFP). *Geoscientific Model Development*, *8*(11), 3695–3713. https://doi.org/10.5194/gmd-8-3695-2015

Koven, C. D., Lawrence, D. M., & Riley, W. J. (2015). Permafrost carbon- climate feedback is sensitive to deep soil carbon decomposability but not deep soil nitrogen dynamics. *Proceedings of the National Academy of Sciences*, *112*(12), 3752–3757. https://doi.org/10.1073/pnas.1415123112

Li, H., Zhang, F., Li, Y., Wang, J., Zhang, L., Zhao, L., et al. (2016). Seasonal and inter-annual variations in CO_2 fluxes over 10 years in an alpine shrubland on the Qinghai-Tibetan Plateau, China. *Agricultural and Forest Meteorology*, *228*, 95–103. https://doi.org/10.1016/j.agrformet.2016.06.020

Li, Y., Dong, S., Liu, S., Zhou, H., Gao, Q., Cao, G., et al. (2015). Seasonal changes of CO_2, CH_4 and N_2O fluxes in different types of alpine grassland in the Qinghai-Tibetan Plateau of China. *Soil Biology and Biochemistry*, *80*, 306–314. https://doi.org/10.1016/j.soilbio.2014.10.026

Liu, F., Kou, D., Chen, Y., Xue, K., Ernakovich, J. G., Chen, L., et al. (2021). Altered microbial structure and function after thermokarst formation. *Global Change Biology*, *27*(4), 823–835. https://doi.org/10.1111/gcb.15438

Liu, X., Zhu, D., Zhan, W., Chen, H., Zhu, Q., Hao, Y., et al. (2019). Five-year measurements of net ecosystem CO_2 exchange at a fen in the Zoige peatlands on the Qinghai-Tibetan Plateau. *Journal of Geophysical Research: Atmospheres*, *124*(22), 11803–11818. https://doi.org/10.1029/2019JD031429

Lüers, J., Westermann, S., Piel, K., & Boike, J. (2014). Annual CO_2 budget and seasonal CO_2 exchange signals at a high Arctic permafrost site on Spitsbergen, Svalbard archipelago. *Biogeosciences*, *11*(22), 6307–6322. https://doi.org/10.5194/bg-11-6307-2014

Lund, M., Falk, J. M., Friborg, T., Mbufong, H. N., Sigsgaard, C., Soegaard, H., & Tamstorf, M. P. (2012). Trends in CO_2 exchange in a high Arctic tundra heath, 2000-2010. *Journal of Geophysical Research: Biogeosciences*, *117*(G2), n/a–n/a. https://doi.org/10.1029/2011JG001901

Lupascu, M., Welker, J. M., Seibt, U., Maseyk, K., Xu, X., & Czimczik, C. I. (2014). High Arctic wetting reduces permafrost carbon feedbacks to climate warming. *Nature Climate Change*, *4*(1), 51–55. https://doi.org/10.1038/nclimate2058

Mauritz, M., Bracho, R., Celis, G., Hutchings, J., Natali, S. M., Pegoraro, E., et al. (2017). Nonlinear CO_2 flux response to 7 years of experimentally induced permafrost thaw. *Global Change Biology*, *23*(9), 3646–3666. https://doi.org/10.1111/gcb.13661

McGuire, A. D., Christensen, T. R., Hayes, D., Heroult, A., Euskirchen, E., Kimball, J. S., et al. (2012). An assessment of the carbon balance of Arctic tundra: Comparisons among observations, process models and atmospheric inversions. *Biogeosciences*, *9*(8), 3185–3204. https://doi.org/10.5194/bg-9-3185-2012

Miao, S., Carstenn, S., & Nungesser, M. (2009). *Real world ecology*. Springer. LLC.

Min, E., Wilcots, M. E., Naeem, S., Gough, L., McLaren, J. R., Rowe, R. J., et al. (2021). Herbivore absence can shift dry heath tundra from carbon source to sink during peak growing season. *Environmental Research Letters*, *16*(2), 024027. https://doi.org/10.1088/1748-9326/abd3d0

Natali, S. M., Watts, J. D., Rogers, B. M., Potter, S., Ludwig, S. M., Selbmann, A. K., et al. (2019). Large loss of CO_2 in winter observed across the northern permafrost region. *Nature Climate Change*, *9*(11), 852–857. https://doi.org/10.1038/s41558-019-0592-8

Niu, B., He, Y., Zhang, X., Du, M., Shi, P., Sun, W., & Zhang, L. (2017). CO_2 exchange in an alpine swamp meadow on the central Tibetan plateau. *Wetlands*, *37*(3), 525–543. https://doi.org/10.1007/s13157-017-0888-2

Niu, F., Gao, Z., Lin, Z., Luo, J., & Fan, X. (2019). Vegetation influence on the soil hydrological regime in permafrost regions of the Qinghai-Tibet Plateau, China. *Geoderma*, *354*. https://doi.org/10.1016/j.geoderma.2019.113892

Oechel, W. C., Laskowski, C. A., Burba, G., Gioli, B., & Kalhori, A. A. (2014). Annual patterns and budget of CO_2 flux in an Arctic tussock tundra ecosystem. *Journal of Geophysical Research: Biogeosciences*, *119*(3), 323–339. https://doi.org/10.1002/2013JG002431

Oechel, W. C., Vourlitis, G. L., Hastings, S. J., Zulueta, R. C., Hinzman, L., & Kane, D. (2000). Acclimation of ecosystem CO_2 exchange in the Alaskan Arctic in response to decadal climate warming. *Nature*, *406*(6799), 978–981. https://doi.org/10.1038/35023137

Piao, S., Zhang, X., Wang, T., Liang, E., Wang, S., Zhu, J., & Niu, B. (2019). Responses and feedback of the Tibetan Plateau's alpine ecosystem to climate change. *Chinese Science Bulletin*, *64*(27), 2842–2855. https://doi.org/10.1360/TB-2019-0074

Pirk, N., Sievers, J., Mertes, J., Parmentier, F. J. W., Mastepanov, M., & Christensen, T. R. (2017). Spatial variability of CO_2 uptake in polygonal tundra: Assessing low-frequency disturbances in eddy covariance flux estimates. *Biogeosciences*, *14*(12), 3157–3169. https://doi.org/10.5194/bg-14-3157-2017

Plaza, C., Pegoraro, E., Bracho, R., Celis, G., Crummer, K. G., Hutchings, J. A., et al. (2019). Direct observation of permafrost degradation and rapid soil carbon loss in tundra. *Nature Geoscience*, *12*(8), 627–631. https://doi.org/10.1038/s41561-019-0387-6

Qin, S., Chen, L., Fang, K., Zhang, Q., Wang, J., Liu, F., et al. (2019). Temperature sensitivity of SOM decomposition governed by aggregate protection and microbial communities. *Science Advances*, *5*(7), eaau1218. https://doi.org/10.1126/sciadv.aau1218

Raz-Yaseef, N., Torn, M. S., Wu, Y., Billesbach, D. P., Liljedahl, A. K., Kneafsey, T. J., et al. (2017). Large CO_2 and CH_4 emissions from polygonal tundra during spring thaw in northern Alaska. *Geophysical Research Letters*, *44*(1), 504–513. https://doi.org/10.1002/2016GL071220

Rodenhizer, H., Ledman, J., Mauritz, M., Natali, S. M., Pegoraro, E., Plaza, C., et al. (2020). Carbon thaw rate doubles when accounting for subsidence in a permafrost warming experiment. *Journal of Geophysical Research: Biogeosciences*, *125*(6), e2019JG005528. https://doi.org/10.1029/2019JG005528

Schädel, C., Koven, C. D., Lawrence, D. M., Celis, G., Garnello, A. J., Hutchings, J., et al. (2018). Divergent patterns of experimental and model-derived permafrost ecosystem carbon dynamics in response to Arctic warming. *Environmental Research Letters*, *13*(10), 105002. https://doi.org/10.1088/1748-9326/aae0ff

Schuur, E. A., Bracho, R., Celis, G., Belshe, E. F., Ebert, C., Ledman, J., et al. (2021). Tundra underlain by thawing permafrost persistently emits carbon to the atmosphere over 15 Years of measurements. *Journal of Geophysical Research: Biogeosciences*, *126*(6), e2020JG006044. https://doi.org/10.1029/2020JG006044

Schuur, E. A., Crummer, K. G., Vogel, J. G., & Mack, M. C. (2007). Plant species composition and productivity following permafrost thaw and thermokarst in Alaskan tundra. *Ecosystems*, *10*(2), 280–292. https://doi.org/10.1007/s10021-007-9024-0

Schuur, E. A., McGuire, A. D., Schädel, C., Grosse, G., Harden, J. W., Hayes, D. J., et al. (2015). Climate change and the permafrost carbon feedback. *Nature*, *520*(7546), 171–179. https://doi.org/10.1038/nature14338

Schuur, E. A., Vogel, J. G., Crummer, K. G., Lee, H., Sickman, J. O., & Osterkamp, T. E. (2009). The effect of permafrost thaw on old carbon release and net carbon exchange from tundra. *Nature*, *459*(7246), 556–559. https://doi.org/10.1038/nature08031

Semikhatova, O. A., Ivanova, T. I., & Kirpichnikova, O. V. (2009). Respiration rate of arctic plants as related to the production process. *Russian Journal of Plant Physiology*, *56*(3), 306–315. https://doi.org/10.1134/S1021443709030029

Shen, M., Piao, S., Jeong, S. J., Zhou, L., Zeng, Z., Ciais, P., et al. (2015). Evaporative cooling over the Tibetan Plateau induced by vegetation growth. *Proceedings of the National Academy of Sciences*, *112*(30), 9299–9304. https://doi.org/10.1073/pnas.1504418112

Starr, G., & Oberbauer, S. F. (2003). Photosynthesis of arctic evergreens under snow: Implications for tundra ecosystem carbon balance. *Ecology*, *84*(6), 1415–1420. https://doi.org/10.1890/02-3154

Thornley, J. H., & Johnson, I. R. (1990). *Plant and crop modelling*. Oxford: Clarendon.

Trucco, C., Schuur, E. A., Natali, S. M., Belshe, E. F., Bracho, R., & Vogel, J. (2012). Seven-year trends of CO_2 exchange in a tundra ecosystem affected by long-term permafrost thaw. *Journal of Geophysical Research: Biogeosciences*, *117*(G2), n/a–n/a. https://doi.org/10.1029/2011JG001907

Ueyama, M., Iwata, H., & Harazono, Y. (2014). Autumn warming reduces the CO_2 sink of a black spruce forest in interior Alaska based on a nine-year eddy covariance measurement. *Global Change Biology*, *20*(4), 1161–1173. https://doi.org/10.1111/gcb.12434

USDA, S. (1999). *Soil taxonomy. Agricultural handbook No. 436, SCS, USDA*.

Vickers, D., & Mahrt, L. (1997). Quality control and flux sampling problems for tower and aircraft data. *Journal of Atmospheric and Oceanic Technology*, *14*(3), 512–526. https://doi.org/10.1175/1520-0426(1997)014<0512:qcafsp>2.0.co;2

Virkkala, A. M., Aalto, J., Rogers, B. M., Tagesson, T., Treat, C. C., Natali, S. M., et al. (2021). Statistical upscaling of ecosystem CO_2 fluxes across the terrestrial tundra and boreal domain: Regional patterns and uncertainties. *Global Change Biology*, *27*, 4040–4059. https://doi.org/10.1111/gcb.15659

Webb, E. E., Schuur, E. A., Natali, S. M., Oken, K. L., Bracho, R., Krapek, J. P., et al. (2016). Increased wintertime CO_2 loss as a result of sustained tundra warming. *Journal of Geophysical Research: Biogeosciences*, *121*(2), 249–265. https://doi.org/10.1002/2014JG002795

Wei, D., Qi, Y., Ma, Y., Wang, X., Ma, W., Gao, T., et al. (2021). Plant uptake of CO2 outpaces losses from permafrost and plant respiration on the Tibetan Plateau. *Proceedings of the National Academy of Sciences*, *118*(33), e2015283118. https://doi.org/10.1073/pnas.2015283118

Welker, J. M., Fahnestock, J. T., Henry, G. H., O'Dea, K. W., & Chimner, R. A. (2004). CO_2 exchange in three Canadian High Arctic ecosystems: Response to long-term experimental warming. *Global Change Biology*, *10*(12), 1981–1995. https://doi.org/10.1111/j.1365-2486.2004.00857.x

Wickland, K. P., Jorgenson, M. T., Koch, J. C., Kanevskiy, M., & Striegl, R. G. (2020). Carbon dioxide and methane flux in a dynamic Arctic tundra landscape: Decadal-scale impacts of ice Wedge degradation and Stabilization. *Geophysical Research Letters*, *47*(22), e2020GL089894. https://doi.org/10.1029/2020GL089894

Wilczak, J. M., Oncley, S. P., & Stage, S. A. (2001). Sonic anemometer tilt correction algorithms. *Boundary-Layer Meteorology*, *99*(1), 127–150. https://doi.org/10.1023/A:1018966204465

Wilson, K., Goldstein, A., Falge, E., Aubinet, M., Baldocchi, D., Berbigier, P., et al. (2002). Energy balance closure at FLUXNET sites. *Agricultural and Forest Meteorology*, *113*(1–4), 223–243. https://doi.org/10.1016/S0168-1923(02)00109-0

Wu, Q., Hou, Y., Yun, H., & Liu, Y. (2015). Changes in active-layer thickness and near-surface permafrost between 2002 and 2012 in alpine ecosystems, Qinghai-Xizang (Tibet) Plateau, China. *Global and Planetary Change*, *124*, 149–155. https://doi.org/10.1016/j.gloplacha.2014.09.002

Wu, Q., & Zhang, T. (2010). Changes in active layer thickness over the Qinghai-Tibetan Plateau from 1995 to 2007. *Journal of Geophysical Research: Atmospheres*, *115*(D9). https://doi.org/10.1029/2009JD012974

Yao, T., Xue, Y., Chen, D., Chen, F., Thompson, L., Cui, P., et al. (2019). Recent third pole's rapid warming accompanies cryospheric melt and water cycle intensification and interactions between monsoon and environment: Multidisciplinary approach with observations, modeling and analysis. *Bulletin of the American Meteorological Society*, *100*(3), 423–444. https://doi.org/10.1175/BAMS-D-17-0057.1

Yun, H., Wu, Q., Zhuang, Q., Chen, A., Yu, T., Lyu, Z., et al. (2018). Consumption of atmospheric methane by the Qinghai-Tibet Plateau alpine steppe ecosystem. *The Cryosphere*, *12*(9), 2803–2819. https://doi.org/10.5194/tc-12-2803-2018

Zhang, R., Su, F., Jiang, Z., Gao, X., Guo, D., Ni, J., et al. (2015). An overview of projected climate and environmental changes across the Tibetan Plateau in the 21st century. *Chinese Science Bulletin*, *60*(32), 3036–3047. https://doi.org/10.1360/N972014-01296

Zhang, T., Zhang, Y., Xu, M., Zhu, J., Chen, N., Jiang, Y., et al. (2018). Water availability is more important than temperature in driving the carbon fluxes of an alpine meadow on the Tibetan Plateau. *Agricultural and Forest Meteorology*, *256*, 22–31. https://doi.org/10.1016/j.agrformet.2018.02.027

Zhang, W., Jansson, P. E., Schurgers, G., Hollesen, J., Lund, M., Abermann, J., & Elberling, B. (2018). Process-oriented modeling of a high Arctic tundra ecosystem: Long-term carbon budget and ecosystem responses to interannual variations of climate. *Journal of Geophysical Research: Biogeosciences*, *123*(4), 1178–1196. https://doi.org/10.1002/2017JG003956

Zhou, Y., Guo, D., Qiu, G., Cheng, G., & Li, S. (2001). Geocryology in China. *Permafrost and Periglacial Processes*, *12*(3), 315–322.

Zhu, Q., Iversen, C. M., Riley, W. J., Slette, I. J., & Vander Stel, H. M. (2016). Root traits explain observed tundra vegetation nitrogen uptake patterns: Implications for trait-based land models. *Journal of Geophysical Research: Biogeosciences*, *121*(12), 3101–3112. https://doi.org/10.1002/2016JG003554

Zhu, J., Zhang, F., Li, H., He, H., Li, Y., Yang, Y., et al. (2020). Seasonal and interannual variations of CO_2 fluxes over 10 Years in an Alpine Wetland on the Qinghai-Tibetan plateau. *Journal of Geophysical Research: Biogeosciences*, *125*(11), e2020JG006011. https://doi.org/10.1029/2020JG006011